Bulk amorphous $Al_{85}Ni_{10}Ce_5$ composite fabricated by cold hydro-mechanical pressing of partially amorphous powders

WEI XianShun[1], HUANG YongJiang[1], VEKSHIN BorisSergeevitch[2], KRAPOSHIN ValentinSidorovitch[2] & SHEN Jun[1*]

[1] *School of Materials Science and Engineering, Harbin Institute of Technology, Harbin 150001, China;*
[2] *Material Science Chair, Bauman Moscow State Technical University, Moscow 105005, Russia*

Gas atomized $Al_{85}Ni_{10}Ce_5$ partially amorphous alloy powders were successfully consolidated into bulk alloy specimens with high relative density at room temperature by cold hydromechanical pressing. The consolidated specimens have a high fracture strength of up to 1.1 GPa. Two densification mechanisms are proposed to explain the consolidation process. The viscous flow of the amorphous phase because of local heating facilities the elimination of residual pores.

powder metallurgy, cold hydromechanical pressing, bulk amorphous alloy, Al-Ni-Ce alloy

Over the last few decades Al-based amorphous alloys with high Al concentrations have received considerable attention because of their high strength combined with excellent bending ductility [1–3]. Although Al-based amorphous alloys exhibit remarkable mechanical properties compared to their crystalline counterparts, most of the as-quenched Al-based amorphous alloys can only be obtained by melt spinning in the shape of thin ribbons or by gas atomization in the form of powders. The glass forming ability (GFA) of Al-based amorphous alloys is relatively lower than that of other alloy systems. Only recently, Al-rich bulk metallic glasses with a diameter of 1 mm have been obtained by copper mould casting [4–8]. The size limitation has seriously restricted the practical application of Al-based amorphous alloys. The fabrication of bulk amorphous alloys by consolidating glassy powders has been shown to be an effective way to overcome the size limitation [9–12]. To consolidate amorphous alloy powders with a low GFA and thermal stability into bulk and full dense specimens without compromising their amorphous structure is a difficult task.

The inhomogeneous deformation of an amorphous alloy at room temperature is mainly localized within a few shear bands leading to catastrophic failure. With an increase in temperature to the supercooled liquid region, which is defined by the temperature range between the glass transition temperature T_g and the crystallization temperature T_x, the amorphous alloy exhibits homogeneous deformation and viscous flow [13–16]. Consequently, the amorphous powders are always consolidated in the supercooled liquid region using their viscous flow characteristics by a conventional consolidation method such as vacuum hot pressing [17] and spark plasma sintering (SPS) [18]. Because of the relatively low crystallization temperature of Al-based amorphous alloys, exposure at high temperature usually leads to crystallization. On the other hand, high temperature is necessary to obtain tight powder particle bonding. However, the temperature fluctuation and temperature gradient, which are difficult to control precisely in a conventional consolidation process, may cause crystallization and deteriorate the material's properties [19–21]. To reduce the influence of temperature control precision, amorphous alloys with a wide supercooled liquid region are always used as

powder materials. It is, therefore, necessary to develop a low temperature powder compaction method to consolidate amorphous alloys with a narrow supercooled liquid region.

Recently, high pressure technology has been shown to be promising for the consolidation of nanocrystalline and amorphous alloy powders into a bulk specimen with relatively high density [22–26]. Very recently, a cold hydro-mechanical pressing (CHMP) consolidation method that combines the triaxial compression principle and high pressure technology has been proposed [27]. The CHMP consolidation process is largely dependent on the configuration of the axial compression stress and the radial hydrostatic pressure. As mentioned in previous investigations the gas atomized pure Al crystalline powders can be successfully consolidated into bulk material with full density and high performance at room temperature using CHMP [27]. It is vital to further study the consolidation process for amorphous or partially amorphous alloy powders by CHMP. In this work, a bulk Al-Ni-Ce amorphous composite was successfully consolidated using the CHMP method at room temperature. The microstructure and mechanical properties of the consolidated specimens were also investigated.

1 Experimental

An Al-Ni-Ce ternary alloy with a nominal composition of $Al_{85}Ni_{10}Ce_5$ (at.%) was selected as the powder material [28,29]. $Al_{85}Ni_{10}Ce_5$ alloy powders were fabricated using the gas atomization method. Powders with sizes below 90 µm were selected by sieving. The size distribution of the powders was measured using a LA-920 laser particle size analyzer. The alloy powders were sealed in a rubber mould without degassing and placed at the bottom of the inner channel of the CHMP apparatus. An appropriate amount of liquid was then used to fill the CHMP vessel. The consolidation process was carried out at room temperature under an axial compression stress σ_1 of 5600 MPa and a radial confining pressure σ_2 of 950 MPa. The consolidated specimen had dimensions of 16 mm in diameter and 15 mm in length. The density of the compacted specimen was determined using the Archimedes' principle, which gives a relative density of 99.4%. The thermal properties were examined using a Pyris 1 differential scanning calorimeter (DSC) under high-purity argon flow at a heating rate of 20 K/min. Structural characterization of the gas atomized powders and the compacted specimen were performed by X-ray diffraction (XRD) using a D/MAX-RA diffractometer with a monochromatic Cu K_α radiation source. Scanning electron microscopy (SEM-FEI Quanta 200) and high resolution TEM (HRTEM-TECNAI TF30ST, 300 kV) were used for microstructural observations. TEM specimens were thinned to about 30 µm by mechanical grinding followed by further thinning to a final thickness by twin polishing (Fischione Model 120). The consolidated specimen was cut to com-

pression specimens with dimensions of 3 mm in diameter and 6 mm in length. Uniaxial compression tests were performed using an Instron 5500 mechanical instrument at room temperature with a constant strain rate of $2×10^{-4}$ s^{-1}. An MTS Nanoindenter XP system was used to characterize the nanohardness values of the gas atomized powders and the consolidated specimen. Indentation tests were conducted under a constant loading rate of 0.03 mN/s. Micro-Vickers hardness values were obtained using an HVS-5 Vickers indenter with a load of 4.9 N and a holding time of 10 s.

2 Results

Figure 1(a) shows the typical morphology of gas atomized $Al_{85}Ni_{10}Ce_5$ alloy powders. Most of the powder particles have a spherical shape and a smooth surface. Figure 1(b) shows the backscattered electron image of powder particles with different sizes. Clearly, the microstructure changes with the powder particle size. Particles with a size above 30 µm were fully crystalline and particles less than 15 µm were fully amorphous. The particles between 15–30 µm were
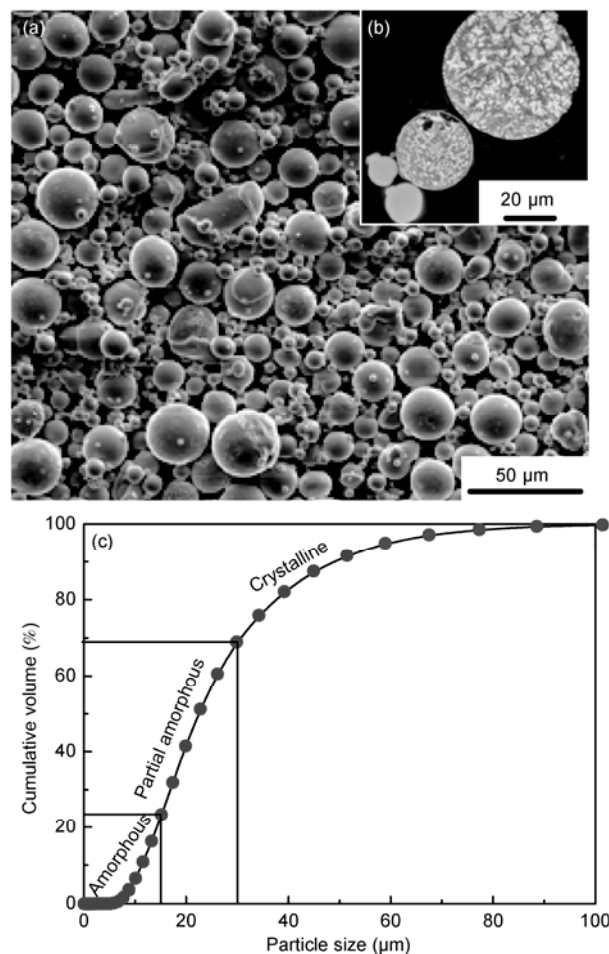

Figure 1 Morphology (a), backscattered electron image (b) and size distribution (c) of the gas atomized $Al_{85}Ni_{10}Ce_5$ alloy powders.

composed of a mixture of crystalline and amorphous phases. The precipitation of dendritic crystalline phases in large particles is due to the low cooling rate of the gas atomization process. The dendritic crystalline phase with bright contrast and the crystalline phase with gray contrast in Figure 1(b) were found to be an Al and Ce enriched phase, and an Al and Ni enriched phase, respectively. The size distribution curve of the gas atomized powders in Figure 1(c) shows that the powder particle size ranges from 5 to 90 μm and the average particle size is 26.9 μm. Additionally, as shown in Figure 1(c), the volume fraction of the fully amorphous particles and the fully crystalline particles are about 23% and 31%, respectively. About half of the gas atomized powders have an amorphous/crystalline composite microstructure.

The XRD patterns of the gas-atomized Al-Ni-Ce alloy powders in Figure 2(a) show a broad halo pattern that is due to the amorphous phase and the sharp Bragg peaks from the crystalline phases, indicating a partially amorphous structure. The XRD pattern of the consolidated specimen in Figure 2(b) also shows an amorphous halo pattern. A decrease in the crystalline phase peak intensity is observed in Figure 2(b). The crystalline products are superimposed on the amorphous phase for the powders and the compacted specimen that is mainly composed of fcc-Al and the intermetallic compounds $Al_{11}Ce_3$, Al_3Ni and τ_6 (Al_5CeNi_2), as generally observed in the Al- rich corner of the Al-Ni-Ce alloy phase diagram [30]. The crystallization products of the gas atomized $Al_{85}Ni_{10}Ce_5$ amorphous powders are slightly different from those of the as-quenched alloy that were annealed at the crystallization temperature [31].

As shown in Figure 3(a), a DSC analysis of the gas atomized powder reveals three exothermic reactions. As reported in previous results, the first exothermic reaction corresponds to the primary crystallization of fcc-Al and an intermetallic compound [32,33]. The glass transition temperature (T_g) and the onset crystallization temperature (T_x) of the gas atomized powder is 526 K and 546 K, respectively. The crystallization behavior of the consolidated specimen is
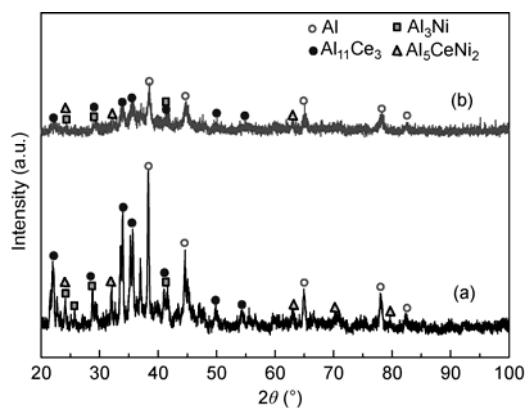

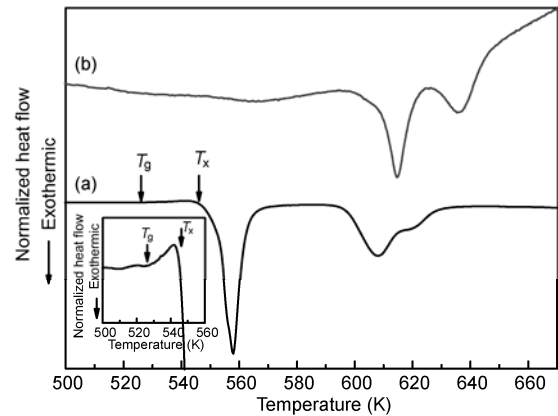**Figure 3**   DSC curves of the gas atomized $Al_{85}Ni_{10}Ce_5$ alloy powders (a) (inset showing an enlarged figure of the supercooled liquid region) and the consolidated specimen (b).

significantly different from that of the gas atomized powders (Figure 3(b)). Unlike the DSC traces obtained from the initial powders, the first exothermic peak of the compacted specimen almost disappeared, and no obvious glass transition temperature was observed, while two distinct exothermic peaks are present at 600 K and at 650 K. The enthalpy of the exothermic peak at 614 K (10.9 J/g) is smaller than that of the initial gas-atomized powders (15.9 J/g).

Figure 4 shows backscattered electron images that were obtained from the longitudinal section of the consolidated specimen. Almost no residual pores or voids exist in the SEM image, which confirms the nearly full density of the consolidated specimens after CHMP consolidation. As shown in Figure 4(a), heavily deformed fully crystalline particles and partially amorphous particles with an ellipse shape dominated the microstructure, and the gaps between these powders were filled with irregular fully amorphous particles. No distinct boundaries are present between the crystalline and the amorphous particles in Figure 4(b) indicating the tight bonding of the particle interface.

The microstructure of the consolidated specimen was also investigated by TEM. Figure 5 shows a bright field image of the consolidated specimen. Four amorphous particles and one crystalline particle are present in Figure 5(a). The discontinuous amorphous powder particle boundaries imply that tight bonding was achieved between the amorphous powders. Shear bands are present at the center (zone marked with the dash-dotted circles in Figure 5(a)) of the amorphous particle. An arrow in the dark-field image (Figure 5(b)) indicates the location where the nanocrystalline phases are present along a shear band at the center region. The selected-area electron diffraction pattern (SAED) (Figure 5(c)) that was taken from the amorphous particle contains diffuse rings that originate from the amorphous phase, indicating that the matrix of this particle is still amorphous after consolidation. Figure 5(d) shows a bright field image that was taken from the crystalline particle in the left corner of Figure 5(a). The region marked with white arrows indicates
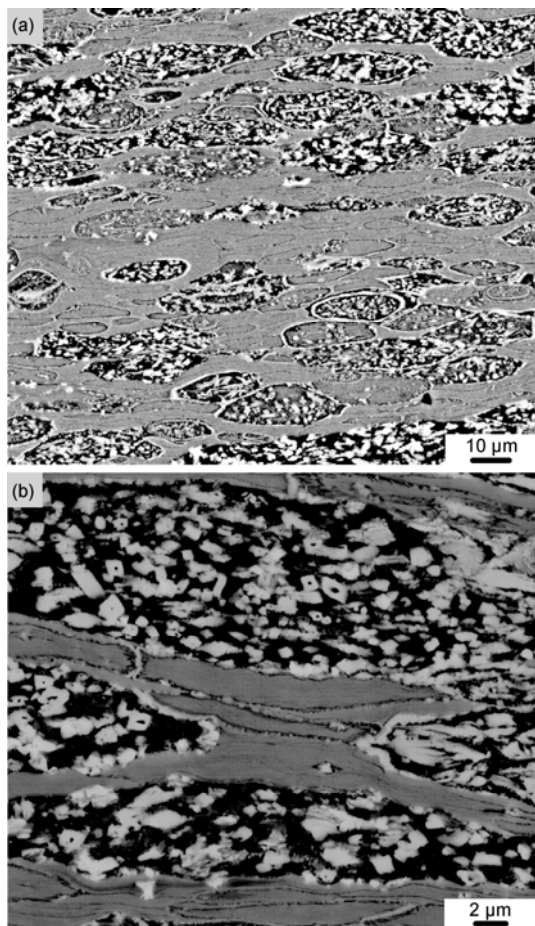

Figure 2   X-ray diffraction patterns of the gas atomized $Al_{85}Ni_{10}Ce_5$ alloy powders (a) and the consolidated specimen (b).

Figure 4 SEM backscattered electron image of the consolidated specimen. (a) Low magnification; (b) high magnification.

Figure 5 TEM bright field image of the consolidated specimen (a), dark-field image (b) and SAED pattern (c) that was obtained from the central (marked with dash-dotted circles in (a) and edge zones of the amorphous particle, and a bright field image (d) with a corresponding SAED pattern (e) that was obtained from the crystalline particle.

Figure 6 Typical compressive stress-strain curves (a), macroscopic fracture morphology (b) and fracture surface of zone I (c) and zone II (d) as obtained from the consolidated specimen.

that cracking occurs in the brittle crystalline phase. The indexing of the SAED pattern for the brittle crystalline phase is shown in Figure 5(e). The diffraction spots along zone axis [011] were found to belong to an orthorhombic-structured τ_6 (CeNi$_2$Al$_5$) intermetallic compound, which agrees with the XRD results in Figure 2. The τ_6 intermetallic compound in the Al-Ni-Ce alloy has attracted much attention because of its unique magnetic properties [34,35].

The mechanical performance of the compacted specimen was characterized by a compression test. Figure 6(a) shows typical stress-strain curves of the consolidated specimen upon uniaxial compression. The fracture strength σ_f and Young's modulus E are 1.1 and 22 GPa, respectively. The fracture strength σ_f of the consolidated specimen is relatively high for the Al-based consolidated specimen [19,36] and the as-cast alloy [4,28]. The Macroscopic fracture morphology of the as-fabricated amorphous composite has two distinct regions, I and II (Figure 6(b)). In region I, the specimen fractured in a pure shear mode and vein patterns (Figure 6(c)) are present at the shear fracture surface. In region II, no individual recognisable particles are observed on the fracture surface (Figure 6(d)), indicating high density and tight particle bonding. The presence of vein patterns in
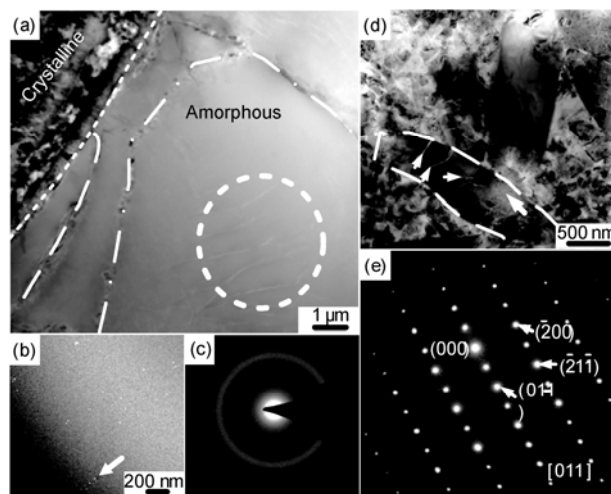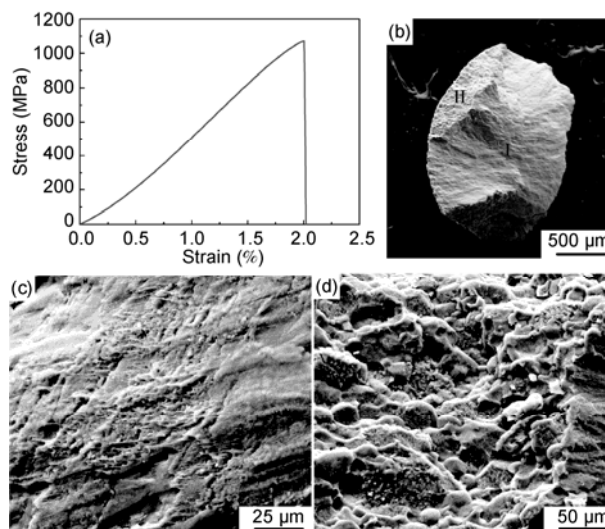
Figure 6(c) is a typical fracture characteristic of Al-based amorphous alloys [28], providing evidence that the amorphous phase is retained after powder consolidation.

Figure 7 shows load-displacement curves that were obtained from indentation tests for the crystalline and amorphous powder particles before and after powder consolidation. The hardness and displacement at maximum load for the crystalline and amorphous powders before and after consolidation are listed in Table 1. As shown in Table 1, before the powder consolidation process, the hardness of the amorphous particles (4.92 GPa) has a larger value than that of crystalline particles (2.85 GPa), therefore, the displacement at maximum load of the amorphous particles (127.44
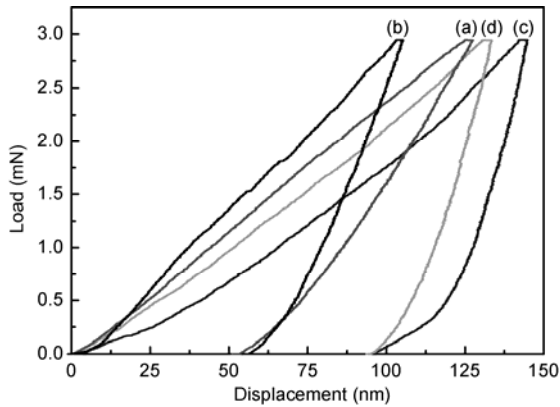
Figure 7 Indentation load-displacement curves of fully amorphous phase particles (a) before and (b) after consolidation, and fully crystalline phase particles (c) before and (d) after consolidation.

Table 1 The modulus, hardness and displacement at maximum load values for the crystalline and amorphous powders before and after consolidation

Powder particle	Consolidation status	Modulus (GPa)	Hardness (GPa)	Displacement at maximum load (nm)
Amorphous	Before	58.34	4.92	127.44
	After	102.23	5.37	105.16
Crystalline	Before	144.54	2.85	144.60
	After	119.09	3.37	133.21

nm) are smaller than that of the crystalline particles (144.60 nm). After powder consolidation by CHMP, the same tendency is observed for the consolidated crystalline, and amorphous particles. The microhardness of the consolidated specimen is 343.5 HV, in accordance with that of the melt spun specimen [37].

3 Discussion

CHMP relies on the combination of high radial hydrostatic pressure and high axial compression stress, which induces enough deformation and material flow of particles, and thus eliminates pores. Figure 8 illustrates the deformation process of the Al-Ni-Ce alloy powders during the CHMP process.
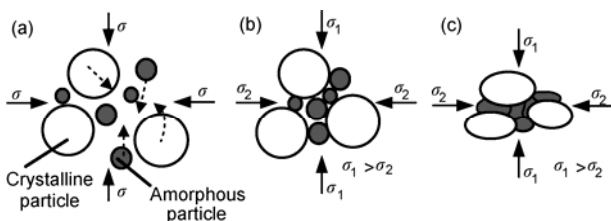

Figure 8 Schematic illustration of the densification process for the partially amorphous alloy powders. (a) Particle rearrangements under isostatic pressure σ during the initial stage, (b) powder consolidation under axial stress σ_1 and radial pressure σ_2, and (c) viscous flow and plastic deformation induced high density consolidation.

During the initial stage of the CHMP process, the applied axial compression stress is equal to the radial pressure, and the powder compact is subjected to an isostatic pressure σ, which is about 250 MPa. The loose initial Al-Ni-Ce alloy powders are then preliminarily compacted into a powder body under isostatic pressure. The dominant densification mechanism in this stage is particle rearrangement by sliding and rotation, therefore, the gaps between the large crystalline particles are filled with small amorphous and semi-amorphous particles (Figure 8(a)). During the final stage of the CHMP process, the upper plunger contacts the upper surface of the powder compact. At this stage the pre-compacted Al-Ni-Ce powder body is subjected to a triaxial compression stress, in which the axial compressive stress σ_1 is larger than the radial pressure σ_2, and shear stress is introduced (Figure 8(b)). Finally the powder particles are consolidated into a bulk specimen with a high relative density (Figure 8(c)). For crystalline powders, the densification mechanism is dominated by yielding and plastic deformation of the powder particles at the contact area. For the partially amorphous Al-Ni-Ce alloy powders, because of the coexistence of crystalline and amorphous particles the densification process is more complicated than that of monolithic particles. From the nanoindentation tests the amorphous particles were found to be harder than the crystalline particles at room temperature. The microstructure of the consolidated specimen in Figure 4 shows that the gaps of the crystalline powders were filled with amorphous particles. These results imply that viscous flow of amorphous phase occurs during the consolidation process. The reason for the viscous flow during the powder consolidation process at room temperature is local heating. After the CHMP process, a temperature increase was observed in the consolidated bulk Al-Ni-Ce powder specimen. The temperature increase for the whole consolidated Al-Ni-Ce specimen was estimated to be 40° and thus the temperature at the particle boundaries may exceed T_g. A temperature increase has also been reported for a high pressure torsion (HPT) process [26]. Local heating is mainly caused by inter-particle friction forces. During the final stage of CHMP the rearrangement of powder particles was confined by the high triaxial pressure. At the hard contact interfaces between the crystalline particles and the amorphous particles, the confined local sliding and rotation was driven by the high shear stress. Therefore, this friction heat results in an increase in temperature in the thin layer on the surface of the amorphous particle when going from room temperature to T_g, which leads to a dramatic decrease in the local viscosity. Because of the local viscous flow, the amorphous particles easily flow into the voids. We found in Figure 5(a) that the viscous flow occurred at the outer layer of the amorphous particle, whereas shear bands appeared in the center of the particle. The reason for the appearance of shear bands is that local heating is not sufficient to heat the centre of the particles to viscous flow conditions, therefore, inhomogeneous defor-

mation occurs in this area. As for warm extrusion, work-induced heat generation may also cause an increase in temperature [38,39]. The ellipse shape of the crystalline particles in Figure 4(b) suggests plastic deformation of the crystalline particles during the consolidation process. Because of work hardening the hardness value of the crystalline particles after consolidation increases (Table 1). The local temperature increases within the crystalline particles because of severe deformation in addition to inter-particle friction may also be responsible for the surface viscous flow of the amorphous particles. Both the viscous flow of the amorphous phases and the plastic deformation of the crystalline phases contribute to the densification process of the powders during the final stage. The viscous flow that results from local heating near the particle boundaries facilitates the achievement of tight particle boundaries and the formation of a consolidated specimen with a high relative density.

In Figure 3(b), the crystallization behavior of the consolidated specimen is significantly distinct from the initial powders. The XRD (Figure 2(b)), SAED (Figure 5(c)) and fracture morphology (Figure 6(c)) results show that the amorphous structure of the initial particles was retained after the CHMP process. It is known that the application of high pressure affects the crystallization behavior of the amorphous alloys [40].

This work shows that at room temperature Al-Ni-Ce alloy powders can be successfully consolidated into a bulk specimen with a high relative density and high performance by the CHMP process. The preservation of the amorphous structure of the particles shows the potential application of CHMP for the consolidation of non-equilibrium structure powder materials.

4 Conclusions

$Al_{85}Ni_{10}Ce_5$ partially amorphous alloy powders were successfully consolidated into a bulk amorphous composite by cold hydromechanical pressing (CHMP). The consolidated specimen has a high density and shows excellent particle bonding as well as a high compressive strength of up to 1.1 GPa. Two mechanisms are proposed to account for the partially amorphous alloy powder densification process; one is particle rearrangement by sliding and rotation at the initial stage, and the other is amorphous viscous flow and crystalline plastic deformation in the final stage.

1   Inoue A, Amiya K, Yoshii I, et al. Production of Al-based amorphous alloy wires with high tensile strength by a melt extraction method. Mater Trans JIM, 1994, 35: 485–488

2   Inoue A. Amorphous, nanoquasicrystalline and nanocrystalline alloys in Al-based systems. Prog Mater Sci, 1998, 43: 365–520

3   Wang E R, Hui X D, Wang S S, et al. Microstructure and mechanical properties of Al-Si-Ni-Ce alloys prepared by gas-atomization spark plasma sintering and hot-extrusion. Mater Sci Eng A, 2011, 528: 5764–5771

4   Mu J, Fu H, Zhu Z, et al. Synthesis and properties of Al-Ni-La bulk metallic glass. Adv Eng Mater, 2009, 11: 530–532

5   Fu H M, Mu J, Wang A M, et al. Synthesis and compressive properties of Al-Ni-Y metallic glass. Phil Mag Lett, 2009, 89: 711–716

6   Yang B J, Yao J H, Chao Y S, et al. Developing Aluminum-based bulk metallic glasses. Phil Mag, 2010, 90: 3215–3231

7   Sun B A, Pan M X, Zhao D Q, et al. Aluminum-rich bulk metallic glasses. Scripta Mater, 2008, 59: 1159–1162

8   Jia R, Bian X F, Lv X Q, et al. The relationship between viscosity and glass forming ability of Al-(Ni)-Yb alloy. Sci China Phys Mech Astron, 2010, 53: 390–393

9   Xie G, Louzguine-Luzgin D V, Li S, et al. Densification of gas atomized Ni-based metallic glassy powders by spark plasma sintering. Mater Trans JIM, 2009, 50: 1273–1278

10 Park E S, Huh M Y, Kim H J, et al. Effect of thickness reduction on consolidation and crystallization of Cu based bulk metallic glass alloy during powder rolling in supercooled liquid region. J Alloys Compd, 2010, 504: 260–263

11 Hsu C, Kai W, Lin H, et al. Fabrication and corrosion behavior of Ti-based bulk metallic glass composites containing carbon nanotubes. J Alloys Compd, 2010, 504: 176–179

12 Kim T, Lee J K, Bae J C. Devitrification behavior and mechanical property of $Cu_{54}Ni_6Zr_{22}Ti_{18}$ glass powders. Mater Lett, 2008, 62: 323–326

13 Lu J, Ravichandran G, Johnson W L. Deformation behavior of the $Zr_{41.2}Ti_{13.8}Cu_{12.5}Ni_{10}Be_{22.5}$ bulk metallic glass over a wide range of strain-rates and temperatures. Acta Mater, 2003, 51: 3429–3443

14 Bae D H, Lim H K, Kim S H, et al. Mechanical behavior of a bulk Cu-Ti-Zr-Ni-Si-Sn metallic glass forming nano-crystal aggregate bands during deformation in the supercooled liquid region. Acta Mater, 2002, 50: 1749–1759

15 Wang G, Shen J, Sun J F, et al. Superplasticity and superplastic forming ability of a Zr-Ti-Ni-Cu-Be bulk metallic glass in the supercooled liquid region. J Non-cryst Solids, 2005, 351: 209–217

16 Chen Q, Liu L, Chan K C. Deformation behavior of Zr-based bulk metallic glass and composite in the supercooled liquid region. Sci China Ser G Phys Mech Astron, 2008, 51: 349–355

17 Kim Y B, Park H M, Jeung W Y, et al. Vacuum hot pressing of gas-atomized Ni-Zr-Ti-Si-Sn amorphous powder. Mater Sci Eng A, 2004, 368: 318–322

18 Shin S, Kim T S, Kang S K. The influence of spark plasma sintering temperature on the mechanical properties and corrosion resistance of $Zr_{65}Al_{10}Ni_{10}Cu_s$ metallic glass powder. Intermetallics, 2010, 18: 2005–2008

19 Noh S J, Jung T K, Kim M S. Fabrication and property of amorphous/nanocrystalline $Al_{84}Ni_{10}Ce_6$ bulk alloy by a powder forging. Mater Sci Forum, 2005, 475-479: 3493–3496

20 Sordelet D J, Rozhkova E, Huang P, et al. Synthesis of $Cu_{47}Ti_{34}$-$Zr_{11}Ni_8$ bulk metallic glass by warm extrusion of gas atomized powders. J Mater Res, 2002, 17: 186–198

21 Robertson J, Im J T, Karaman I, et al. Consolidation of amorphous copper based powder by equal channel angular extrusion. J Non-cryst Solids, 2003, 317: 144–151

22 Yavari A R, Filho W J B, Rodrigues C A D, et al. Nanostructured bulk $Al_{90}Fe_5Nd_5$ prepared by cold consolidation of gas atomised powder using severe plastic deformation. Scripta Mater, 2002, 46: 711–716

23 Roy D, Mitra R, Chudoba T, et al. Structure and mechanical properties of $Al_{65}Cu_{20}Ti_{15}$-based amorphous/nanocrystalline alloys prepared by high-pressure sintering. Mater Sci Eng A, 2008, 497: 93–100

24 Gutmanas E Y, Rabinkin A, Roitberg M. Cold sintering under high pressure. Scripta Mater, 1979, 13: 11–15

25 Bobrovnitchii G S, Holanda J N F. Cold consolidation of ATR-Niobium

powder under high pressure. J Mater Process Tech, 2005, 170: 187–191

26 Vierke J, Schumacher G, Pilyugin V P, et al. Deformation-induced crystallization in amorphous $Al_{85}Ni_{10}La_5$ alloy. J Alloy Compd, 2010, 493: 683–691

27 Wei X S, Vekshin B, Kraposhin V, et al. Full density consolidation of pure Aluminium powders by cold hydromechanical pressing. Mater Sci Eng A, 2011, 528: 5784–5789

28 Inoue A, Amiya K, Yoshii I, et al. Production of Al-based amorphous alloy wires with high tensile strength by a melt extraction method. Mater Trans JIM, 1994, 35: 485–488

29 Cochrane R F, Schumacher P, Greer A L. Crystallization of amorphous $Al_{85}Ni_{10}Ce_5$ alloy. Mater Sci Eng A, 1991, 133: 367–370

30 Tang C, Du Y, Wang J, et al. Correlation between thermodynamics and glass forming ability in the Al-Ce-Ni system. Intermetallics, 2010, 18: 900–906

31 Sha P, Qi Z, Zhang Z. Effect of Ag or Pd additions on the microstructure, crystallization and thermal stability of Al-Ni-Ce amorphous alloys. Intermetallics, 2010, 18: 1699–1706

32 Tsai A P, Kamiyama T, Kawamura Y, et al. Formation and precipitation mechanism of nanoscale Al particles in Al-Ni base amorphous alloys. Acta Mater, 1997, 45: 1477–1487

33 Wang S H, Bian X F. Effect of Si and Co on the crystallization of Al-Ni-Re amorphous alloys. J Alloy Compd, 2008, 453: 127–130

34 Nakashima M, Tabata K, Thamizhavel A, et al. High-pressure effect on the electrical resistivity in $CeNiGe_3$ and $CeNi_2Al_5$. Physica B, 2005, 359-361: 266–268

35 Isikawa Y, Akamaru S, Mizushima T, et al. Precise magnetization measurement and magnetostriction of dense-kondo compound $CeNi_2Al_5$. J Magn Magn Mater, 2001, 226-230: 205–207

36 Senkov O N, Miracle D B, Scott J M, et al. Equal channel angular extrusion compaction of semi-amorphous $Al_{85}Ni_{10}Y_{2.5}La_{2.5}$ alloy powder. J Alloy Compd, 2004, 365: 126–133

37 Muoz-Morris M A, Suriach S, Varga L K, et al. The influence of composition and low temperature annealing on hardness and ductility of rapidly solidified Al-Ni-Ce alloys. Scripta Mater, 2002, 47: 31–37

38 Kawamura Y, Kato H, Inoue A, et al. Full strength compacts by extrusion of glassy metal powder at the supercooled liquid state. Appl Phys Lett, 1995, 67: 2008–2010

39 Kawamura Y, Inoue A, Sasamori K, et al. Consolidation mechanism of Aluminum-based amorphous alloy powders during warm extrusion. Mater Sci Eng A, 1994, 181-182: 1174–1178

40 Krasnowski M, Antolak-Dudka A, Kulik T. Bulk amorphous $Al_{85}Fe_{15}$ alloy and $Al_{85}Fe_{15}$-B composites with amorphous or nanocrystalline-matrix produced by consolidation of mechanically alloyed powders. Intermetallics, 2011, 19: 1243–1249